Realization of a Periodically Driven Open Three-Level Dicke Model

Phatthamon Kongkhambut,[1] Hans Keßler,[1,*] Jim Skulte,[1,2] Ludwig Mathey,[1,2]
Jayson G. Cosme,[3] and Andreas Hemmerich[1,2]
[1]Zentrum für Optische Quantentechnologien and Institut für Laser-Physik, Universität Hamburg, 22761 Hamburg, Germany
[2]The Hamburg Center for Ultrafast Imaging, Luruper Chaussee 149, 22761 Hamburg, Germany
[3]National Institute of Physics, University of the Philippines, Diliman, Quezon City 1101, Philippines

(Received 26 August 2021; accepted 2 November 2021; published 13 December 2021)

A periodically driven open three-level Dicke model is realized by resonantly shaking the pump field in an atom-cavity system. As an unambiguous signature, we demonstrate the emergence of a dynamical phase, in which the atoms periodically localize between the antinodes of the pump lattice, associated with an oscillating net momentum along the pump axis. We observe this dynamical phase through the periodic switching of the relative phase between the pump and cavity fields at a small fraction of the driving frequency, suggesting that it exhibits a time crystalline character.

DOI: 10.1103/PhysRevLett.127.253601

Rapid technological advances have elevated cold-atom systems to preeminent platforms for realizing model systems of quantum–many body dynamics [1–6]. An intriguing subclass is hybrid light-matter systems, which are composed of cold atoms coupled to an optical cavity, and display a strongly enhanced light-matter interaction, giving access to the physics of strong light-matter coupling and long-range correlations [7,8]. A specific feature of these platforms is the well controlled dissipation, which allows for fast nondestructive *in situ* monitoring of the system dynamics [8–15]. One of the fundamental models for light-matter interaction is the Dicke model [16,17]. It describes a collection of N two-level systems coupled to a single light mode and displays a phase transition between a normal and a superradiant phase [16]. An open version of the Dicke model with a weak dissipation channel is approximately realized by a Bose-Einstein condensate (BEC) placed in a linear standing wave optical cavity and pumped by an optical standing wave oriented perpendicularly with respect to the cavity axis [10,11,15,18–26]. The normal phase is characterized by a BEC, light shifted by the pump potential, with a homogeneous density distribution along the cavity axis and a small number of photons in the cavity that do not display coherence. The superradiant phase shows a density grating enabling pronounced scattering of photons from the pump into the cavity and vice versa. Various extensions of the standard two-level Dicke model have been proposed and realized using atom-cavity systems, such as the spin-1 Dicke model [27,28] and the two-component Dicke model [29–31], all sharing the coupling of two-level systems to the same monochromatic light mode.

The extension of the Dicke model to the case of three-level systems has been theoretically considered in Refs. [32–34]. A specific example in a ring cavity has been used to experimentally demonstrate subradiance [35]. In the present work, we experimentally realize the periodically driven open three-level Dicke model by shaking the standing wave pump potential in an atom-cavity system as depicted in Fig. 1(a). It has been predicted in Ref. [36] that this enables a dynamical phase, characterized by atoms periodically localizing between the antinodes of the pump lattice, i.e., on the intersite bonds, which has been called dynamical bond density wave (DBDW) phase. This DBDW phase exhibits time crystalline character and is a characteristic signature of the periodically driven open three-level Dicke model. Its experimental observation is the central topic of this work.

We define the three-level Dicke model to describe the interaction between a single quantized light mode and N three-level atoms comprising energy eigenstates $|1\rangle$, $|2\rangle$, and $|3\rangle$ in a V configuration. Its Hamiltonian is

$$H/\hbar = \omega\hat{a}^\dagger\hat{a} + \omega_{12}\hat{J}_z^{12} + \omega_{13}\hat{J}_z^{13} + \frac{2}{\sqrt{N}}(\hat{a}^\dagger + \hat{a})(\lambda_{12}\hat{J}_x^{12} + \lambda_{13}\hat{J}_x^{13}). \quad (1)$$

The bosonic operator $\hat{a}$ ($\hat{a}^\dagger$) annihilates (creates) a photon with frequency ω. The frequency detuning between the lowest energy state $|1\rangle$ and the other two states $|2\rangle$ and $|3\rangle$ are ω_{12} and ω_{13}, respectively. For small detuning ω_{23} between the states $|2\rangle$ and $|3\rangle$, i.e., when $\omega_{23} \ll \omega_{12}, \omega_{13}$, the only relevant light-matter interactions are those that couple state $|1\rangle$ with states $|2\rangle$ and $|3\rangle$, the strengths of which are given by λ_{12} and λ_{13}, respectively. We introduce the pseudospin operators $\hat{J}_\mu^\ell$ with $\ell \in \{12, 13, 23\}$, which are related to the eight generators of the SU(3) group [37]. Note that the Gell-Mann matrices, the standard representation of the SU(3) group, can be obtained by an appropriate superposition of $\hat{J}_\mu^\ell$ [37]. Equation (1) is an extended

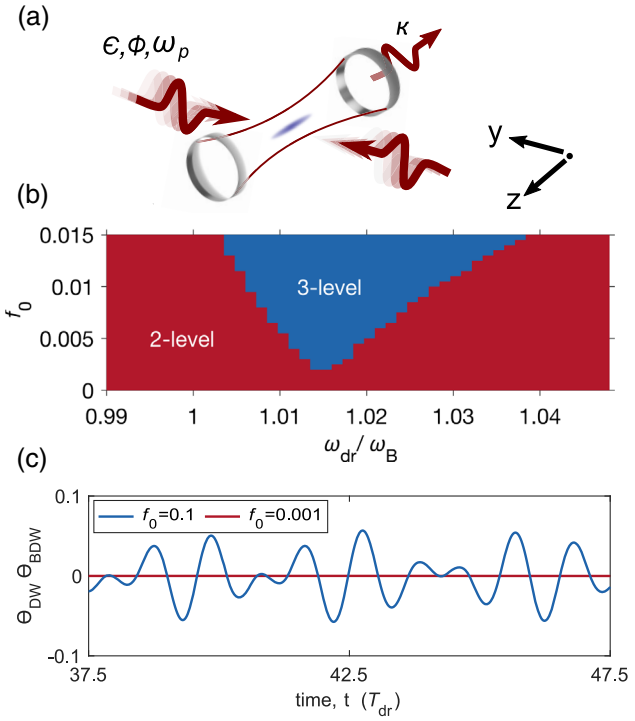

FIG. 1. (a) Schematic of the transversely pumped and shaken atom-cavity system. A sample of cold atoms is placed in a cavity oriented along the z axis. A standing wave potential is periodically shifted along the y axis using phase modulation techniques. (b) Dynamical phase diagram with two distinct regions: In the red area, the dynamics of the system is captured by a two-level Dicke model. In the blue area, a three-level Dicke model is required. (c) Dynamics of the product of the relevant order parameters for strong driving in the three-level Dicke regime (blue) and for weak driving in the two-level Dicke regime (red). The modulation frequency is $\omega_{\rm dr}/2\pi = 9.4$ kHz and $\omega_B/2\pi = 8$ kHz.

form of the two-component Dicke model [29–31]. However, the latter obeys the SU(2) algebra, while the pseudospin operators in Eq. (1) fulfill the SU(3) algebra, instead.

To implement the three-level Dicke model, we consider atoms in their electronic ground state occupying the following three momentum states forming a V-shaped level structure (see Fig. 1 in Supplemental Material [38]). The ground state is the so called BEC state $|\mathrm{BEC}\rangle$ given by the zero momentum state $|0,0\rangle$ with respect to the yz plane, light shifted by the pump field by an amount $-\epsilon/2$, where ϵ denotes the potential depth of the pump wave [37]. The first excited state is the superposition $\sum_{\nu,\mu\in\{-1,1\}} |\nu\hbar k, \mu\hbar k\rangle$ of the four momentum modes $|\pm\hbar k, \pm\hbar k\rangle$ associated with the yz plane, light shifted by the pump field by an amount $-3\epsilon/4$ (here, k denotes the wave number of the pump field) [37]. In view of its spatially varying density $\propto |\cos(ky)\cos(kz)|^2$, it is denoted as the density wave state $|\mathrm{DW}\rangle$. The light shift for $|\mathrm{DW}\rangle$ is larger compared to that of $|\mathrm{BEC}\rangle$, since the density distribution of $|\mathrm{DW}\rangle$ is localized in the antinodes of the pump field [37]. The two states $|\mathrm{BEC}\rangle$ and $|\mathrm{DW}\rangle$ span the matter sector of the regular two-level Dicke model. If ϵ exceeds a critical value $\epsilon_{\rm crt}$, $|\mathrm{BEC}\rangle$ acquires an admixture of $|\mathrm{DW}\rangle$. A Bragg grating is thus imprinted upon the density of the $|\mathrm{BEC}\rangle$ state, which via efficient scattering of pump light builds up a coherent intracavity light field. The $|\mathrm{BEC}\rangle$ state, thus dressed by the cavity field, is denoted superradiant phase. In this work, we operate either with $\epsilon < \epsilon_{\rm crt}$ or with ϵ only very slightly above $\epsilon_{\rm crt}$, such that the additional dressing by the cavity field is zero or negligibly small. The second excited state is associated with the momentum state superposition $\sum_{\nu,\mu\in\{-1,1\}} \nu|\nu\hbar k, \mu\hbar k\rangle$. This state exhibits the smallest light shift $-\epsilon/4$, because its density distribution $\propto |\sin(ky)\cos(kz)|^2$ matches with the nodes of the pump wave [37]. This state is called bond density wave (abbreviated $|\mathrm{BDW}\rangle$) as its density maxima coincide with the bonds between two potential minima of the pump wave. We denote the energy separation between $|\mathrm{DW}\rangle$ and $|\mathrm{BEC}\rangle$ as $\hbar\omega_D$, and that between $|\mathrm{BDW}\rangle$ and $|\mathrm{BEC}\rangle$ as $\hbar\omega_B$, respectively. See Supplemental Material for a more detailed description [38].

In the atom-cavity implementation of the standard Dicke model, $|\mathrm{BDW}\rangle$ is not coupled to $|\mathrm{BEC}\rangle$ and hence can be dropped. To implement a coupling between $|\mathrm{BDW}\rangle$ and $|\mathrm{BEC}\rangle$, the transverse pump lattice is periodically shaken in space [36]. In Ref. [37], we show that the Hamiltonian for the shaken atom-cavity system can be mapped onto a parametrically driven version of the three-level Dicke model.

$$H/\hbar = \omega\hat{a}^\dagger\hat{a} + \hat{J}_z^D\omega_D + \hat{J}_z^B\omega_B + 2\phi(t)(\omega_B - \omega_D)\hat{J}_x^{DB} + \frac{2\lambda}{\sqrt{N}}(\hat{a}^\dagger + \hat{a})[\hat{J}_x^D - \phi(t)\hat{J}_x^B], \tag{2}$$

where $\phi(t) = f_0\sin(\omega_{\rm dr}t)$ is the time-dependent spatial phase of the pump lattice introduced by the shaking protocol, and λ is the overall coupling strength parameter. The pseudospin operators $\hat{J}_\mu^D$ and $\hat{J}_\mu^B$ with $\mu \in \{x, y, z\}$ are directly associated with the $|\mathrm{DW}\rangle$ and the $|\mathrm{BDW}\rangle$ states via the relations to their order parameters $\Theta_{\rm DW} \equiv \langle\cos(ky)\cos(kz)\rangle = \langle\hat{J}_x^D\rangle$ and $\Theta_{\rm BDW} \equiv \langle\sin(ky)\cos(kz)\rangle = \langle\hat{J}_x^B\rangle$, respectively. Comparing Eqs. (1) and (2), we identify $\hat{J}_\mu^{12} = \hat{J}_\mu^D$, $\hat{J}_\mu^{13} = \hat{J}_\mu^B$, $\hat{J}_\mu^{23} = \hat{J}_\mu^{DB}$, $\omega_{12} = \omega_D$, $\omega_{13} = \omega_B$, $\lambda_{12} = \lambda$, and a time-dependent light-matter coupling $\lambda_{13} = -\phi(t)\lambda$. Moreover, in Eq. (2), the standing wave potential of the pump introduces an additional albeit negligible term proportional to $\hat{J}_x^{DB}$, which couples $|\mathrm{DW}\rangle$ and $|\mathrm{BDW}\rangle$ [37].

For driving frequencies $\omega_{\rm dr}$ slightly above ω_B, the DBDW phase shows periodic oscillations of $\Theta_{\rm BDW}$ and $\Theta_{\rm DW}$ around zero with frequencies $\omega_{\rm BDW}$ and $\omega_{\rm DW}$, respectively. Theory predicts the relation $\omega_{\rm DW} = \omega_{\rm dr} - \omega_{\rm BDW}$ such that $\omega_{\rm DW}$ is not an integer fraction of the driving frequency $\omega_{\rm dr}$ [36]. This is a hallmark of an incommensurate time crystal [36].

Thus, the long-time average of Θ_{DW} is zero in the three-level Dicke region of the dynamical phase diagram, while it is nonzero in the two-level Dicke region for an initial superradiant phase. This behavior is captured in Fig. 1(b), which shows the time-averaged value of $\langle \hat{J}_x^D \rangle / N \equiv j_x^D$ obtained by solving the equations of motion corresponding to Eq. (2) in the semiclassical limit of a large atom number [37].

The DBDW dynamics may be experimentally studied via the product of the order parameters $\Theta_{\mathrm{DW}} \times \Theta_{\mathrm{BDW}}$, which can be approximately measured by the normalized occupation imbalance $\Delta\tilde{F} \equiv (F_{+1,\pm1} - F_{-1,\pm1})/(F_{+1,\pm1} - F_{-1,\pm1})_{\max}$, where $F_{\pm1,\pm1}$ denotes the population of the momentum state $|\pm\hbar k, \pm\hbar k\rangle$ (see Supplemental Material for details [38]). In the standard Dicke model realized for off-resonant driving, $\Theta_{\mathrm{BDW}} \approx 0$ and $\Delta\tilde{F}$ is negligible. On the other hand, for driving frequencies ω_{dr} slightly above ω_B, a beating signal is expected in $\Theta_{\mathrm{DW}} \times \Theta_{\mathrm{BDW}}$ [see Fig. 1(c)], which can be observed via $\Delta\tilde{F}$. Furthermore, the periodic switching of Θ_{DW} in the three-level model amounts to a periodic switching of the experimentally observable relative phase of the pump and the cavity fields $\varphi \equiv \arg(\langle \hat{a} \rangle)$ between 0 and π.

In our experiment, a BEC of ^{87}Rb atoms is superimposed with the fundamental mode of a high-finesse optical cavity pumped by a retroreflected laser beam at wavelength $\lambda_P = 803$ nm. The resulting optical pump lattice has a depth ϵ and is aligned perpendicular to the cavity axis, as depicted in Fig. 1(a). The cavity has a field decay rate $\kappa = 2\pi \times 3.6$ kHz comparable to the recoil frequency $\omega_{\mathrm{rec}} \equiv \hbar k^2/2m$ ($m =$ atomic mass), such that the cavity field and the atomic density distribution evolve on similar timescales. This leads to a retarded infinite-range cavity-mediated interaction between the atoms [13]. The system realizes the Dicke phase transition from a homogeneous BEC to a superradiant phase if ϵ exceeds a critical strength. The $\mathbb{Z}_2$ symmetry is spontaneously broken, when the atoms localize at either the even or odd sites of a two dimensional checkerboard optical lattice formed by the interference between the pump and intracavity fields. The two symmetry broken states can be distinguished by the relative phase difference φ between the pump and intracavity light fields using a balanced heterodyne detection of the cavity field. The appearance of the superradiant phase can be detected *in situ* by the observation of a nonzero cavity mode occupation N_P [see red line in Fig. 2(b)], the locking of the relative φ to zero or π [see green line Fig. 2(b)], or in a destructive way through a nonzero occupation of the $\{p_y, p_z\} = \{\pm\hbar k, \pm\hbar k\}$ modes in a momentum spectrum [see Fig. 2(g)].

The experimental sequence proceeds as follows. We prepare the system in the BEC phase or in the superradiant phase close to the phase boundary towards the BEC phase, followed by a 500 μs long waiting period to let the system reach its steady state. Then, we shake the pump potential by modulating the phase of the pump field using an

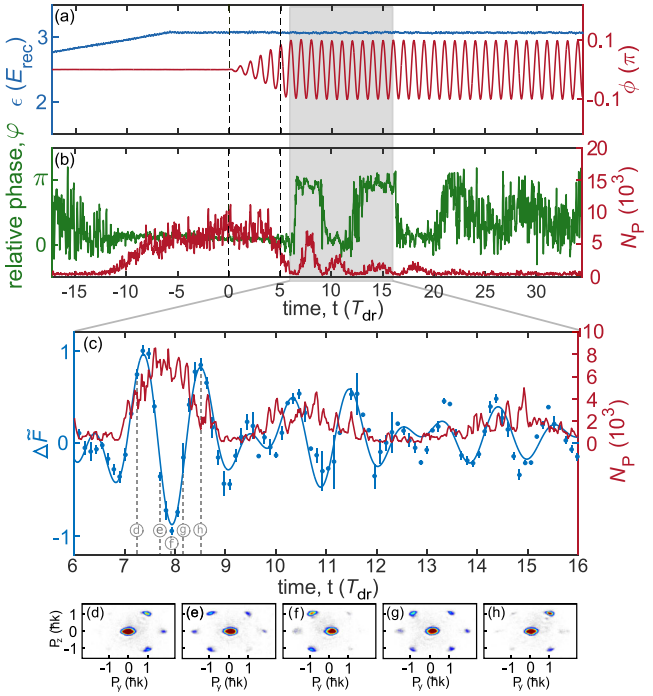

FIG. 2. Single-shot realization of DBDW order. (a) Time sequence for the pump lattice depth (blue) and the phase ϕ of the pump field (red) with modulation strength $f_0 = 0.1\pi$ and a modulation frequency $\omega_{\mathrm{dr}} = 11.5$ kHz. (b) Phase difference φ between the pump and intracavity field (green trace) and photon number N_P in the cavity (red trace). The dashed vertical lines mark the time interval during which the modulation strength is increased. The gray shaded area shows the time window for the close-up presented in (c). (c) The red trace repeats the intracavity photon number N_P from (b). The blue data points plot the product $\Theta_{\mathrm{DW}} \times \Theta_{\mathrm{BDW}}$, approximately given by $\Delta\tilde{F}$ [see also Fig. 1(c)]. Each data point is averaged over five realizations. The solid line shows a fit with a product of two harmonic oscillations. (d)–(h) Single-shot momentum distributions recorded at the times marked in (c).

electro-optical modulator. The modulation strength f_0 is linearly increased to its desired value within 500 μs and kept constant for 6.5 ms. A typical sequence of the pump protocol is presented in Fig. 2(a). Resonant driving induces a switching of the system between the two possible sublattices of the superradiant phase at a frequency ω_{DW} and the intracavity photon number pulsates at a rate of $2\omega_{\mathrm{DW}}$. This behavior is exemplified in the green and red curves in Fig. 2(b).

In Fig. 3(a), we plot ω_{DW} as a function of ω_{dr} and average each data point over 100 experimental runs including different modulation strength f_0. The solid gray trace shows a linear fit. We find good agreement with the theoretical prediction $\omega_{\mathrm{DW}} = \omega_{\mathrm{dr}} - \omega_{\mathrm{BDW}}$ of Ref. [36]. In Supplemental Material, we present a similar plot for fixed ω_{dr} and varying f_0 to show that the dependence of ω_{DW} on f_0 is very weak and negligible within the experimental precision [38]. From the linear fit in Fig. 3(a),

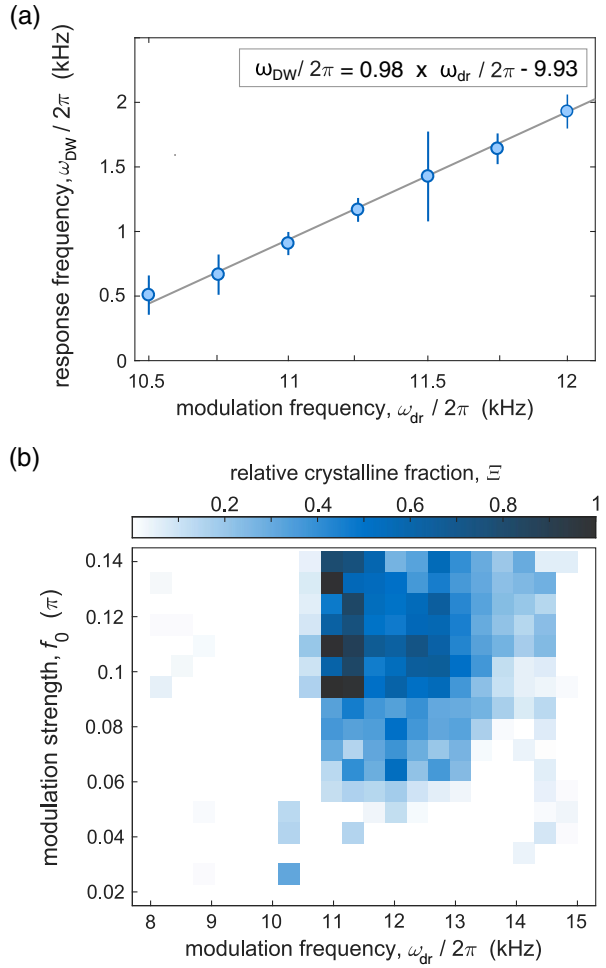

FIG. 3. (a) ω_{DW} is plotted against ω_{dr}. ω_{DW} is extracted by the position of a Gaussian fit of the amplitude spectrum calculated from the measured time evolution of the phase difference between the pump and cavity fields φ. Each data point is averaged over hundreds of realizations with different modulation strength f_0 and fixed ω_{dr}. The gray line is a linear fit yielding the result shown in the plot legend. (b) The relative crystalline fraction Ξ is plotted as a function of the modulation frequency ω_{dr} and strength f_0. The diagram is constructed by dividing the parameter space into 20×16 plaquettes and averaging over multiple experimental runs within each.

we extract the value of the parametric resonance as $\omega_{\mathrm{BDW}} = 9.93 \pm 0.30$ kHz. In Supplemental Material, we also present an alternative protocol for measuring ω_{BDW} from the depletion of the cavity field for resonant modulation [38]. In Fig. 3(b), we present the dynamical phase diagram, highlighting the DBDW order obtained from measuring the relative crystalline fraction Ξ quantified by the color scale. The relative crystalline fraction is a quantity commonly used in studies of time crystals. Here, we define it as the amplitude of the Fourier spectrum, calculated from the relative phase φ, at the expected DW frequency ω_{DW}, rescaled by its maximum value across the parameter space spanned in the phase diagram [15]. The observed DW frequency follows the linear equation $\omega_{\mathrm{DW}} = \xi \times \omega_{\mathrm{dr}} - \omega_{\mathrm{BDW}}$ with ξ determined according to the linear fit in Fig. 3(a) as 0.98, i.e., very close to the expected value of unity. This incommensurate subharmonic response of the system with respect to the modulation frequency ω_{dr} is observed within a broad area of the dynamical phase diagram in Fig. 3(b). In Supplemental Material, we present the robustness of the subharmonic response against temporal noise, which corroborates the classification of this dynamical phase as an incommensurate time crystal.

Finally, we discuss the observed dynamics of the momentum imbalance parameter $\Delta\tilde{F}$ related to the calculations in Fig. 1(c). The oscillation frequencies ω_{DW} and ω_{BDW} are extracted from the data in Fig. 2(c) using $f(t) = \exp(-\tau t)A\sin(\omega_{\mathrm{BDW}}t + \alpha)\sin(\omega_{\mathrm{DW}}t)$ as a fit function. Here, τ is the decay rate of N_P and A is an overall amplitude parameter. This measurement demonstrates a third option for measuring ω_{BDW}. However, since recording the momentum spectra is a destructive measurement, this method is much more time consuming than simply detecting the light leaking out of the cavity, which makes it extremely difficult to explore large areas in the parameter space. Nevertheless, we repeated this measurement for a second set of modulation parameters shown in Supplemental Material [38]. The frequency ω_{BDW} is independent of ω_{dr} and we measure $\omega_{\mathrm{BDW}} = 2\pi \times 9.8 \pm 0.1$ kHz. For a driving frequency of $\omega_{\mathrm{dr}} = 11.5$ kHz, we measure a slow oscillation frequency of $\omega_{\mathrm{DW}} = 2\pi \times 1.8 \pm 0.1$ kHz [see Fig. 2(c)], which agrees well with the theoretical prediction of $\omega_{\mathrm{DW}} = \omega_{\mathrm{dr}} - \omega_{\mathrm{BDW}} = 2\pi \times (11.5 - 9.8)$ kHz $= 2\pi \times 1.7$ kHz.

While we have mostly focused on the case when initially the superradiant state is prepared, we have also confirmed that it is possible to enter the three-level regime heralded by the emergence of the DBDW phase by initializing with the homogeneous BEC or normal phase as exemplified in Fig. 4.

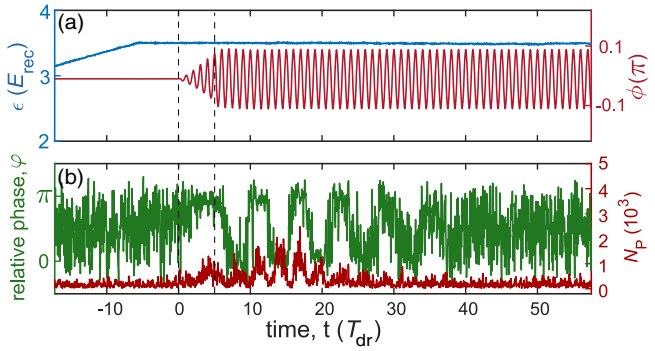

FIG. 4. Dynamics in the three-level Dicke regime using an initial homogeneous BEC state. (a) Time sequence for the pump lattice depth (blue) and the phase ϕ of the pump field (red) with modulation strength $f_0 = 0.1\pi$ and a modulation frequency $\omega_{\mathrm{dr}} = 11.5$ kHz. (b) The phase difference φ between the pump and intracavity field is plotted in green and the photon number N_P in the cavity in red.

The finite lifetime of the emergent DBDW phase in our experiment can be mainly attributed to atom losses. Furthermore, we note that our numerical simulations indicate that contact interactions [36] and larger detunings $\omega_{\mathrm{dr}} - \omega_B$ [38] decrease the lifetime of the time crystalline response. In the experiment, however, it is difficult to quantitatively separate the effects of atom losses, contact interaction, and detuning from the resonance.

In conclusion, we have realized a periodically driven open three-level Dicke model using a resonantly shaken atom-cavity system. As the main signature of the three-level Dicke model, we have demonstrated the emergence of a dynamical bond density wave phase. When prepared in the three-level Dicke regime, our system realizes an incommensurate time crystal, whereby the atoms periodically self-organize along the bonds of the pump lattice. This advances the understanding of cavity-BEC systems beyond the standard two-level Dicke model, and broadens the scope of dynamically induced many-body states in this and related hybrid light-matter systems.

We thank G. Homann and L. Broers for useful discussions. This work is funded by the Deutsche Forschungsgemeinschaft (DFG, German Research Foundation) SFB-925 Project No. 170620586 and the Cluster of Excellence Advanced Imaging of Matter (EXC 2056), Project No. 390715994. J. S. acknowledges support from the German Academic Scholarship Foundation.

*Corresponding author.
hkessler@physnet.uni-hamburg.de

[1] I. Bloch, J. Dalibard, and W. Zwerger, Many-body physics with ultracold gases, Rev. Mod. Phys. **80**, 885 (2008).
[2] I. Bloch, Quantum gases, Science **319**, 1202 (2008).
[3] W. S. Bakr, J. I. Gillen, A. Peng, S. Fölling, and M. Greiner, A quantum gas microscope for detecting single atoms in a Hubbard-regime optical lattice, Nature (London) **462**, 74 (2009).
[4] I. Bloch, J. Dalibard, and S. Nascimbène, Quantum simulations with ultracold quantum gases, Nat. Phys. **8**, 267 (2012).
[5] C. Gross and I. Bloch, Quantum simulations with ultracold atoms in optical lattices, Science **357**, 995 (2017).
[6] L. Bayha, M. Holten, R. Klemt, K. Subramanian, J. Bjerlin, S. M. Reimann, G. M. Bruun, P. M. Preiss, and S. Jochim, Observing the emergence of a quantum phase transition shell by shell, Nature (London) **587**, 583 (2020).
[7] H. Ritsch, P. Domokos, F. Brennecke, and T. Esslinger, Cold atoms in cavity-generated dynamical optical potentials, Rev. Mod. Phys. **85**, 553 (2013).
[8] F. Mivehvar, F. Piazza, T. Donner, and H. Ritsch, Cavity QED with quantum gases: New paradigms in many-body physics, Adv. Phys. **70**, 1 (2021).
[9] A. T. Black, H. W. Chan, and V. V. Vuletic, Observation of Collective Friction Forces due to Spatial Self-Organization of Atoms: From Rayleigh to Bragg Scattering, Phys. Rev. Lett. **91**, 203001 (2003).
[10] K. Baumann, R. Mottl, F. Brennecke, and T. Esslinger, Exploring Symmetry Breaking at the Dicke Quantum Phase Transition, Phys. Rev. Lett. **107**, 140402 (2011).
[11] J. Klinder, H. Keßler, M. Wolke, L. Mathey, and A. Hemmerich, Dynamical phase transition in the open Dicke model, Proc. Natl. Acad. Sci. U.S.A. **112**, 3290 (2015).
[12] H. Keßler, J. Klinder, B. P. Venkatesh, C. Georges, and A. Hemmerich, In situ observation of optomechanical Bloch oscillations in an optical cavity, New J. Phys. **18**, 102001 (2016).
[13] J. Klinder, H. Keßler, C. Georges, J. Vargas, and A. Hemmerich, Bose-Einstein condensates in an optical cavity with sub-recoil bandwidth, Appl. Phys. B **122**, 299 (2016).
[14] C. Georges, J. Vargas, H. Keßler, J. Klinder, and A. Hemmerich, Bloch oscillations of a Bose-Einstein condensate in a cavity-induced optical lattice, Phys. Rev. A **96**, 063615 (2017).
[15] H. Keßler, P. Kongkhambut, C. Georges, L. Mathey, J. G. Cosme, and A. Hemmerich, Observation of a Dissipative Time Crystal, Phys. Rev. Lett. **127**, 043602 (2021).
[16] K. Hepp and E. H. Lieb, On the superradiant phase transition for molecules in a quantized radiation field: The dicke maser model, Ann. Phys. (N.Y.) **76**, 360 (1973).
[17] P. Kirton, M. M. Roses, J. Keeling, and E. G. Dalla Torre, Introduction to the Dicke model: From equilibrium to nonequilibrium, and *vice versa*, Adv. Quantum Technol. **2**, 1800043 (2019).
[18] D. Nagy, G. Szirmai, and P. Domokos, Self-organization of a Bose-Einstein condensate in an optical cavity, Eur. Phys. J. D **48**, 127 (2008).
[19] K. Baumann, C. Guerlin, F. Brennecke, and T. Esslinger, Dicke quantum phase transition with a superfluid gas in an optical cavity, Nature (London) **464**, 1301 (2010).
[20] M. P. Baden, K. J. Arnold, A. L. Grimsmo, S. Parkins, and M. D. Barrett, Realization of the Dicke Model Using Cavity-Assisted Raman Transitions, Phys. Rev. Lett. **113**, 020408 (2014).
[21] F. Piazza and H. Ritsch, Self-Ordered Limit Cycles, Chaos, and Phase Slippage with a Superfluid inside an Optical Resonator, Phys. Rev. Lett. **115**, 163601 (2015).
[22] A. U. J. Lode and C. Bruder, Fragmented Superradiance of a Bose-Einstein Condensate in an Optical Cavity, Phys. Rev. Lett. **118**, 013603 (2017).
[23] H. Keßler, J. G. Cosme, M. Hemmerling, L. Mathey, and A. Hemmerich, Emergent limit cycles and time crystal dynamics in an atom-cavity system, Phys. Rev. A **99**, 053605 (2019).
[24] P. Molignini, L. Papariello, A. U. J. Lode, and R. Chitra, Superlattice switching from parametric instabilities in a driven-dissipative Bose-Einstein condensate in a cavity, Phys. Rev. A **98**, 053620 (2018).
[25] H. Keßler, J. G. Cosme, C. Georges, L. Mathey, and A. Hemmerich, From a continuous to a discrete time crystal in a dissipative atom-cavity system, New J. Phys. **22**, 085002 (2020).
[26] C. Georges, J. G. Cosme, H. Keßler, L. Mathey, and A. Hemmerich, Dynamical density wave order in an atom-cavity system, New J. Phys. **23**, 023003 (2021).
[27] Z. Zhiqiang, C. H. Lee, R. Kumar, K. J. Arnold, S. J. Masson, A. S. Parkins, and M. D. Barrett, Nonequilibrium

phase transition in a spin-1 Dicke model, Optica **4**, 424 (2017).
[28] S. J. Masson, M. D. Barrett, and S. Parkins, Cavity QED Engineering of Spin Dynamics and Squeezing in a Spinor Gas, Phys. Rev. Lett. **119**, 213601 (2017).
[29] E. I. Rodríguez Chiacchio and A. Nunnenkamp, Dissipation-Induced Instabilities of a Spinor Bose-Einstein Condensate inside an Optical Cavity, Phys. Rev. Lett. **122**, 193605 (2019).
[30] B. Buča and D. Jaksch, Dissipation Induced Nonstationarity in a Quantum Gas, Phys. Rev. Lett. **123**, 260401 (2019).
[31] N. Dogra, M. Landini, K. Kroeger, L. Hruby, T. Donner, and T. Esslinger, Dissipation-induced structural instability and chiral dynamics in a quantum gas, Science **366**, 1496 (2019).
[32] C. C. Sung and C. M. Bowden, Phase transition in the multimode two- and three-level Dicke model (Green's function method), J. Phys. A **12**, 2273 (1979).
[33] A. Crubellier, S. Liberman, D. Pavolini, and P. Pillet, Superradiance and subradiance: I. Interatomic interference and symmetry properties in three-level systems, J. Phys. B **18**, 3811 (1985).
[34] A. Crubellier and D. Pavolini, Superradiance and subradiance: II. Atomic systems with degenerate transitions, J. Phys. B **19**, 2109 (1986).
[35] P. Wolf, S. C. Schuster, D. Schmidt, S. Slama, and C. Zimmermann, Observation of Subradiant Atomic Momentum States with Bose-Einstein Condensates in a Recoil Resolving Optical Ring Resonator, Phys. Rev. Lett. **121**, 173602 (2018).
[36] J. G. Cosme, J. Skulte, and L. Mathey, Time crystals in a shaken atom-cavity system, Phys. Rev. A **100**, 053615 (2019).
[37] J. Skulte, P. Kongkhambut, H. Keßler, A. Hemmerich, L. Mathey, and J. G. Cosme, companion paper, Parametrically driven dissipative three-level Dicke model, Phys. Rev. A **104**, 063705 (2021).
[38] See Supplemental Material at http://link.aps.org/supplemental/10.1103/PhysRevLett.127.253601 for details on the experimental setup, the three-level scheme, dependence of the density wave frequency on modulation strength, measurement of parametric resonance using the depletion of intracavity field, and robustness against temporal noise of the dynamical BDW phase.